Time reversal optimization for underwater communications

António Silva[1 a)], Sérgio M. Jesus[1] and João Gomes[2]

[1]*Institute for Systems and Robotics, Universidade do Algarve, Campus de Gambelas, PT-8005-139 Faro, Portugal*

[2]*Institute for Systems and Robotics, Instituto Superior Técnico, Av. Rovisco Pais, 1049-001 Lisboa, Portugal*

Submitted: JASA, 20 of April, 2007

Received:

Running title: Time reversal optimization for underwater communications

[b)]Electronic mail: asilva@ualg.pt

Abstract

Passive time reversal is one of the variants of time reversal applicable to digital underwater communications. In passive time reversal a probe-signal is transmitted ahead of the data-signal in order to estimate the channel impulse response for later use as a replica signal in a time reversal mirror fashion. In practice the received probe-signal must be captured in a time window and, after correlation with the transmitted probe-signal, give a noisy estimation of the channel impulse response. Therefore, the output signal to noise ratio (SNR) and the detection rate of passive time reversal will strongly depend of the starting time and on the duration of such time window. Typically the beginning and the duration of that time window should depend on the transit time and the dispersion of the acoustic channel. Heuristic reasoning would suggest that if a short time window fails to include all significant multipath it will result in an imperfect focusing, while a too long time window will reduce the efficiency of the communication system by introducing additional noise in the passive time reversal system. That problem clearly calls for an optimization. In order to bring the time reversal capabilities to a practical modem the time window automatic optimization engineering problem must be solved. In this paper, the maximization of the passive time reversal output SNR relative to the probe time window was obtained in a closed form. Theoretical results are found to be in full coincidence with simulations and with results obtained on experimental data taken during the INTIFANTE'00 sea trial.

PACS numbers: 43.60 (Ac,Dh,Fg,Gk,Tj)
Keywords: Coherent underwater acoustic communications, shallow water propagation, acoustic time-reversal.

I. Introduction

In the past few years coherent modulation techniques for fast and reliable shallow water acoustic communication have triggered a number of theoretic developments, simulations and field experiments. To that end multichannel adaptive equalization methods [1], although quite computationally demanding, currently provide the most popular framework. Recently, active and passive Time Reversal (a-pTR) [2, 3] appeared as a viable alternative for simple and robust underwater coherent communications [4, 5, 6]. Active Time Reversal (aTR) takes advantage of the acoustic channel mode orthogonality and reciprocity properties and matches the ocean response with itself in a much similar way as in Matched Field Processing (MFP)[7]. Likewise aTR, passive Time Reversal (pTR) relies on mode orthogonality but instead of the reciprocity property, uses an estimate of the underwater channel Green's function to perform a virtual ocean response match inside the computer, in a MFP fashion. Despite its simplicity, a-pTR applied to high frequency underwater communications always presents a lower performance than multichannel equalization [8, 9, 10]. That is due to the Time Reversal Mirror (TRM) requirement for a long and dense array [11], without which a residual Inter-Symbol Interference (ISI) always remains due to a poor sampling of the high order modes and subsequent orthogonality property violation.

One of the most critical aspects of the a-pTR methods is the channel Green's function estimation, which is typically obtained by simply convolving the received channel distorted probe-signal with the transmitted one, resulting in a noisy version of the channel Impulse Response (IR). In practice the probe-signal can be a M-sequence, a chirp, or the pulse shape adopted in the data digital modulation. In any case, and since the underwater channel is quite time variable, probe-signals must be frequently transmitted in order to maintain the a-pTR performance in an acceptable level. A significantly different technique is to adaptively estimate the channel Green's function by using the data communication signal [12], in a

similar manner to that used in the multichannel equalizer [1] with, however, the difference that the IR must be estimated instead of its inverse. As in the multichannel equalizer, such technique is computationally very demanding when compared with the probe-signal based Green's function estimation.

Figure 1 shows a block diagram of the pTR application adopted in the sequel, where the received probe-signal $f'_k(t)$ is the channel IR estimate that is simply obtained as the channel noise contaminated response to a dirac impulse (upper path in the block diagram). For later use the estimated IR must be approximated by a FIR filter, which means that it must be captured in a finite time window (see figure 1). Typically, the start time and the duration of such time window should depend on the time dispersion of the acoustic channel which, in turn, depends on the physical channel properties and on the experiment geometry. Heuristic reasoning would suggest that if a short time window fails to include all significant multipath it will result in an imperfect retrofocusing, while a too long time window will reduce the efficiency of the communication system and introduce additional noise in the pTR operation [5, 8, 13].

The time window probe-signal capture optimization is an important issue, since it will strongly affect the pTR Inter-symbolic Interference (ISI), the output Signal-to-Noise Ratio (SNR) and thus the detection error rate. Time window optimization can be transformed in a problem of pTR output SNR maximization, that can be solved after establishing signal and noise power time window dependence. The a-pTR output SNR have been addressed by several authors [10, 14], including heuristic characterizations of time window dependence [5, 8, 13] thought optimization was not attempted.

In section II. a closed form expression for the pTR output SNR as a function of the time window is obtained and strategies for its optimization are proposed. In particular, it is found that the optimal time window does not depend on the noise level but only on the multipath structure of the underwater acoustic channel. Section III. presents the results

obtained in simulation using realistic underwater acoustic propagation models. In section IV. the proposed optimization method will be applied to real data acquired during the INTIFANTE'00 sea trial. The conclusions and future work are presented in section V.

II. Theoretical background

The objective of this section is to set up the theoretical background for analysing the implications of probe-signal windowing operation in pTR performance when applied to digital communications in presence of acoustic noise. Since time-reversal recombines energy as a matched filter, whose function is to maximize the output SNR at a given time instant [10], time windowing optimization can be obtained from a closed form expression for the pTR otput SNR. It is found that the optimum time window corresponds to the pTR output SNR maximum, which depends solely on the multipath structure of the underwater channel.

A. Digital communications with passive Time Reversal

Figure 1 shows the baseband equivalent of the source-channel-receiver representation of the pTR processor for one hydrophone. In a first step (upper path in figure 1) a duly time windowed and phase conjugated channel IR estimate is computed. In the second step (lower path in figure 1) the deconvolution of the transmitted data sequence a_n distorted by the underwater channel is accomplished using the estimated channel IR computed in the first step. In that figure, the transmitting and receiving filter, $p(t)$, is a fourth-root raised cosine pulse [1]. In the sequel

$$p_m(t) = \underbrace{p(t) * ... * p(t)}_{\text{m times}}, \tag{1}$$

represents the m-times self-convolution of $p(t)$ such that $p_4(t)$ is the raised-cosine pulse shape function. In the IR estimation step, $p_2(t)$ is used as a narrowband filter resulting in a square-

[1] for notation convenience it is assumed that $p(t)$ is the inverse Fourier transform of $\sqrt[4]{P_4(f)}$, where $P_4(f)$ is a raised cosine pulse in the frequency domain.

root raised cosine shape. In the second step $p(t)$ is used as the transmitting pulse shape for the data sequence that, in conjunction with $p(t)$ in the receiver side, results in a received data sequence square-root raised cosine pulse shaped, distorted with the baseband equivalent channel IR $h_k(t)$. With such configuration, in presence of a non-distortive channel (that is $h_k(t) = h'_k(t) = \delta(t)$) and with a sufficiently large time window, one can guarantee a raised cosine pulse shape for the data sequence in the pTR output signal $z_k(t)$.

Let us assume that the transmitted signal is Pulse Amplitude Modulated (PAM) written as

$$s(t) = a(t) * p(t), \tag{2}$$

with

$$a(t) = \sum_{n=-\infty}^{+\infty} a_n \delta(t - nT_b), \tag{3}$$

where a_n is a zero mean symbol sequence assumed to be white with power σ_a^2, and T_b is the symbol duration.

Assuming the acoustic channel as a time-invariant linear system with impulse response $h_k(t)$, the received data-signal at hydrophone k is given by

$$v_k(t) = h_k(t) * a(t) * p_2(t) + w_k(t) * p(t), \tag{4}$$

where $w_k(t)$ is an additive zero mean white noise with power σ_w^2, assumed to be uncorrelated with the signal and from sensor to sensor. When the probe-signal is a dirac impulse the received signal (upper path in figure 1) is written as

$$f'_k(t) = h'_k(t) + u_k(t) \tag{5}$$

where $u_k(t)$ is the channel additive noise sequence with the same properties as $w_k(t)$ and independent from it, $h'_k(t)$ is the same channel impulse response as $h_k(t)$ (no environment/geometry mismatch case) and the $'$ denotes that there is an unspecified time delay between the two impulse responses (IRs).

The time window operator multiplies the input signal with a unit-gate function of length τ and starting point t_0 (A4), thus

$$f'_{k,t_0,\tau}(t) = \begin{cases} f'_k(t), & t \in [t_0, t_0+\tau]; \\ 0, & \text{elsewhere} \end{cases}. \tag{6}$$

The narrowband time-limited IR estimate is then obtained as

$$g_{k,t_0,\tau}(t) = f'_{k,t_0,\tau}(t) * p_2(t). \tag{7}$$

Finally, the time limited IR estimation is phase conjugated or, equivalently in the time domain, time-reversed and conjugated. The pTR output for channel k is therefore

$$z_k(t) = g^*_{k,t_0,\tau}(-t) * v_k(t) \tag{8}$$

where $v_k(t)$ is given by (4). Replacing (3), (4) and (7) in (8) and summing over the hydrophone index k, the pTR output signal can be written as

$$z(t) = y(t) + x1(t) + x2(t) + x3(t), \tag{9}$$

where $y(t)$ contains the desired data-signal contaminated with ISI and the other three terms are noise disturbances, defined as

$$\begin{aligned} y(t) &= \sum_{n=-\infty}^{+\infty} a_n c(t - nT_b) \\ x1(t) &= \sum_{n=-\infty}^{+\infty} a_n e(t - nT_b) \\ x2(t) &= p_3(t) * \sum_{k=1}^{K} h^*_{k,t0,\tau}(-t) * w_k(t) \\ x3(t) &= p_3(t) * \sum_{k=1}^{K} u^*_{k,t0,\tau}(-t) * w_k(t), \end{aligned} \tag{10}$$

where

$$\begin{aligned} c(t) &= p_4(t) * \sum_{k=1}^{K} h_k(t) * h^*_{k,t0,\tau}(-t) \\ e(t) &= p_4(t) * \sum_{k=1}^{K} h_k(t) * u^*_{k,t0,\tau}(-t). \end{aligned} \tag{11}$$

The next logic step will be to derive the pTR output SNR using (9) and proceed to its maximization relative to the time window parameters t_0 and τ, respectively start time and duration. Before doing so, and in order to motivate this optimization procedure, figures 2 and 3 anticipate the results obtained, respectively in simulation (section III.) and with real data (section IV.). The depth dependent IRs are shown for a reduced time scale where the sign 'o' indicates the time window starting instant t_0, sign '*' indicates the optimum time window duration, the one that guarantees the pTR best performance $t_0 + \tau_{opt}$ as derived from the optimization of the output SNR, and sign '+' indicate the maximum time window duration considered in the analysis, $t_0 + \tau_{max}$. Close inspection reveals that as the time window increases, more IR paths are included in $h_{k,t_0,\tau}(t)$ and simultaneously more noise power is included in $u_{k,t_0,\tau}(t)$. Those two factors will affect the pTR performance in opposite directions, resulting in an optimum time window that does not include all the arriving paths ('*' signs). It should be noted however that, in order for the system to operate as a pTR, the time windowing operation must contain at least the main arrivals of the channel IRs. When operating with a vertical line array this can be done by using the same time window for all hydrophones since at long ranges, greater than a few water depths, the main arrivals approximate plane waves. Under those conditions t_0 must be set before the main arrivals and τ must be large enough to include all relevant paths. In order to proceed to the output SNR maximization one needs to first derive the various noise cross terms that will appear in the SNR expression denominator.

B. Autocorrelation of the noise terms

In order to obtain a closed form expression for the pTR SNR output it is important to characterize each noise disturbance $x1 \ldots 3$ individually, namely by determining their mean and variance. Their mean is easily calculated since the additive noise is zero mean, then $E\{x1 \ldots 3(t)\} = 0$. The variance can be obtained as the value of the autocorrelation function

at the origin after demonstrating that the noise terms are zero-mean Wide Sense Stationary (WSS).

The autocorrelation function of $x_3(t)$ can be obtained considering that the autocorrelation of the convolution is equal to the convolution of the autocorrelations and that the autocorrelation of a sum is the sum of the autocorrelation plus the cross correlated terms that will be null for independent summation terms. Assuming the independence of noise from sensor to sensor, and (A8), the autocorrelation of $x3$ will be

$$\begin{aligned} R_{x3}(t+t',t) &= E\{x3(t+t')x3(t)\} \\ &= r_{p_3}(t') * \sigma_w^2\sigma_u^2\tau K r_\delta(t') \\ &= r_{p_3}(t')\sigma_w^2\sigma_u^2\tau K \\ &= R_{x3}(t'), \end{aligned} \tag{12}$$

where σ_w^2 and σ_u^2 are the noise variances of $w(t)$ and $u(t)$ respectively, τ is the window length, K is the number of hydrophones, $r_{p_3}(t')$ is the autocorrelation of $p_3(t)$ and $r_\delta(t')$ is the autocorrelation of $\delta(t)$. In order to compute its variance it is important to note that $x3(t)$ is a WSS stochastic signal.

For $x_2(t)$ the autocorrelation can be computed considering (A8) and (A12) for each hydrophone k,

$$\begin{aligned} R_{x2,k}(t+t',t) &= E\{x2_k(t+t')x2_k(t)\} \\ &= r_{p_3}(t') * r_{h,k,t_0,\tau}(t') * \sigma_w^2\delta(t') \\ &= r_{p_3}(t') * r_{h,k,t_0,\tau}(t')\sigma_w^2 \\ &= R_{x2,k}(t'). \end{aligned} \tag{13}$$

Thus, since the autocorrelation of the sum over the entire array is the sum of the autocorrelations given by (13) plus the cross-correlation terms that are null due to the noise

independence from sensor to sensor, the autocorrelation of $x_2(t)$ is given by

$$R_{x2}(t') = r_{p_3}(t') * \sigma_w^2 \sum_{k=1}^{K} r_{h,k,t_0,\tau}(t'). \tag{14}$$

This equation can be further simplified considering that for a well positioned time window that covers the most significant paths of $h_k(t)$, according to the TRM basic principle associated assumptions [2], and considering (A11)

$$\sum_{k=1}^{K} r_{hk,t_0,\tau}(t') \approx C_{x2}(t_0,\tau)\delta(t'), \tag{15}$$

with the time window dependent coefficient

$$C_{x2}(t_0,\tau) \approx \sum_{k=1}^{K} \int_{t_0}^{t_0+\tau} h_k(t) h_k^*(t) dt, \tag{16}$$

where $C_{x2}(\cdot)$ is a baseband version of C' from (A22).

Thus the autocorrelation of $x2(t)$ is approximately equal to

$$\begin{aligned} R_{x2}(t') &\approx r_{p_3}(t') * \sigma_w^2 C_{x2}(t_0,\tau)\delta(t') \\ &\approx r_{p_3}(t')\sigma_w^2 C_{x2}(t_0,\tau), \end{aligned} \tag{17}$$

which means that $x2$ is also a WSS stochastic signal.

For the autocorrelation of $x1(t)$, the signal will be considered as the convolution of two continuous stochastic signals

$$x1(t) = a(t) * e(t), \tag{18}$$

where $a(t)$ and $e(t)$ are respectively given in (3) and (11). The autocorrelation of $e(t)$ is obtained by applying (A19) to the summation terms $h_k(t) * u^*_{k,t0,\tau}(-t)$, and by applying (A3)

$$\begin{aligned} R_e(t+t',t) &= \int\int r_{p_4}(t'-\gamma)\sigma_u^2 C_{x1}(\gamma,\nu,\tau) d\nu d\gamma \\ &= \sigma_u^2 \int r_{p_4}(t'-\gamma) \int C_{x1}(\gamma,\nu,\tau) d\nu d\gamma, \end{aligned} \tag{19}$$

[2] *i.e.*, that there is a sufficiently large number of hydrophones, the vertical array is spanning whole the water column and the propagation environment is time-invariant.

where $C_{x1}(\cdot,\cdot,\cdot)$ is a summation of terms analogous to $A_\tau(\cdot,\cdot,z=0)$ given in (A18), that is

$$C_{x1}(t',t,\tau)=\sum_{k=1}^{K}\int_{t-\tau}^{t}h_k(\lambda+t')h_k^*(\lambda)d\lambda. \tag{20}$$

In (20) the integral is given by

$$\begin{aligned}\int_{-\infty}^{+\infty}C_{x1}(t',t,\tau)dt &= \int_{-\infty}^{+\infty}\sum_{k=1}^{K}\int_{t-\tau}^{t}h_k(\alpha+t')h_k(\alpha)d\alpha dt\\ &= \sum_{k=1}^{K}\int_{-\infty}^{+\infty}\int_{-\infty}^{+\infty}h_k(\alpha+t')h_k(\alpha)\Pi_{t-\tau,\tau}(\alpha)d\alpha dt\\ &= \sum_{k=1}^{K}\int_{-\infty}^{+\infty}h_k(\alpha+t')h_k(\alpha)\int_{-\infty}^{+\infty}\Pi_{t-\tau,\tau}(\alpha)dtd\alpha\\ &= \tau\sum_{k=1}^{K}\int_{-\infty}^{+\infty}h_k(\alpha+t')h_k(\alpha)d\alpha\\ &\approx \tau C_h\delta(t'),\end{aligned} \tag{21}$$

where $\Pi_{t-\tau,\tau}(\alpha)$ is an unit-gate sliding window, similar to (A4) with constant area equal to τ, and

$$C_h=\sum_{k=1}^{K}\int h_k(t)h_k^*(t)dt, \tag{22}$$

by considering analogous assumptions as those for $x2(t)$. In (22) C_h is a baseband version of C in (A21). The autocorrelation of $e(t)$ will be given by

$$R_e(t+t',t)=R_e(t')=r_{p_4}(t')\sigma_u^2\tau C_h, \tag{23}$$

where $e(t)$ becomes a WSS stochastic signal.

The PAM signal $a(t)$ is a cyclostationary signal [15, 16] given by (3), but here the strategy used in [15] will be adopted whereby $a(t)$ is changed to $a(t)=\sum_{n=-\infty}^{+\infty}a_n\delta(t+\Theta-nT_b)$, where Θ is an unknown timing phase that reflects the fact that the origin of the time axis is arbitrary. By considering that Θ is uniformly distributed over the interval $[0,T_b[$, $a(t)$ becomes WSS with autocorrelation given by

$$R_a(t')=\frac{\sigma_a^2}{T_b}r_\delta(t'), \tag{24}$$

where $r_\delta(t')$ is the autocorrelation of the dirac impulse. Finally, the autocorrelation of $x_1(t)$ can be seen as the convolution of the autocorrelations of $e(t)$ and $a(t)$, and is given by

$$R_{x1}(t') = r_{p_4}(t')\frac{\sigma_a^2}{T_b}\sigma_u^2 C_h \tau, \tag{25}$$

where one can see that $x_1(t)$ is also WSS.

C. Signal and noise power

In order to compute the pTR output SNR (SNR_{out}) the signal and the noise terms power must be obtained. Since we have already computed the noise terms autocorrelation and shown that they are zero mean WSS processes, their power can be easily computed by considering its variance equal to the autocorrelation at the origin

$$\sigma_{x3}^2(\tau) = R_{x3}(0) = r_{p_3}(0)\sigma_w^2\sigma_u^2\tau K, \tag{26}$$

$$\sigma_{x2}^2(t_0,\tau) = R_{x2}(0) = r_{p_3}(0)\sigma_w^2 C_{x2}(t_0,\tau), \tag{27}$$

$$\sigma_{x1}^2(\tau) = R_{x1}(0) = r_{p_4}(0)\frac{\sigma_a^2}{T_b}\sigma_u^2 C_h \tau. \tag{28}$$

In (9) the PAM data-signal has pulse shape $c(t)$ given by (11), and considering similar assumptions to those underlying (24) its power is

$$\sigma_y^2(t_0,\tau) = \frac{\sigma_a^2}{T_b}[C_y(t_0,\tau)]^2 r_{p_4}(0), \tag{29}$$

where $C_y(t_0,\tau)$ is computed in a similar manner to $C_{x2}(t_0,\tau)$ and becomes

$$\begin{aligned} C_y(t_0,\tau)\delta(t') &\approx \sum_{k=1}^{K}\int_{-\infty}^{\infty} h_k(t+t')h_{k,t_0,\tau}^*(t)dt \\ &\approx \sum_{k=1}^{K}\int_{t_0}^{t_0+\tau} h_k(t+t')h_k^*(t)dt. \end{aligned} \tag{30}$$

Under those conditions $[C_y(t_0,\tau)]^2$ is the autocorrelation at the origin of $C_y(t_0,\tau)\delta(t')$, and $C_y(.)$ is a baseband version of C'' in (A23).

In the above equations the time window dependent factors $C_{\cdot}(.)$ that affect the signal and noise power terms are equivalent to TRM gains at the focal point for different configurations of the channel IRs limited and/or unlimited. Such constants are related with each other and it is important to note that when TRM associated assumptions are fulfilled C_{x2} is equal to C_y and as τ increases they both converge to C_h.

D. The pTR output SNR and its maximum

The signal and noise power terms have already been found in (26), (27), (28) and (29). Since $x1$, $x2$ and $x3$ are zero mean independent random terms the variance of the sum is simply the sum of the variances and the pTR ouptut SNR will be given by

$$SNR_{out}(t_0,\tau) = \frac{\sigma_y^2(t_0,\tau)}{\sigma_{x3}^2(\tau) + \sigma_{x2}^2(t_0,\tau) + \sigma_{x1}^2(\tau)}, \tag{31}$$

where its dependence on the window length, τ, and starting time t_0 is perfectly clear.

After the pTR operation, the data frame detection can be made, as in figure 1, in two steps: by sampling the pTR output signal $z(t)$ at a the symbol period, T_b, that will result in the sampled signal $z(nT_b)$ corrupted by noise and ISI, followed by a slicer/detector that estimates the transmitted symbols one by one. Since the TR operator recombines energy as a matched filter, whose function is to maximize the SNR and not to eliminate the ISI [10], the pTR output SNR given by equation (31) considers that the TR residual ISI is part of the signal and not a corruption term. Such intrinsic residual ISI of the TR operator depends on the environment properties and receiving array configuration, and although it can be reduced by using an extremely dense array that spans all the water column, it can not be eliminated. For digital communications purpose the residual ISI should be considered as a corruption term similar to a noise term and that will result in a different pTR output SNR computed by using the MSE at the detector input [10, 16]

$$SNR_{mse}(t_0,\tau) = \frac{1}{MSE(t_0,\tau)} - 1. \tag{32}$$

When the output noise power is dominant $SNR_{out}(t_0,\tau) \approx SNR_{mse}(t_0,\tau)$, but when ISI dominates SNR_{mse} saturates while the SNR_{out} increases as the noise power decreases. In spite of the differences between the SNR_{out} given in (31) and SNR_{mse} given in (32), their maxima occur for the same time window duration, which will be clarified in section III.. Window parameters for optimal detection can therefore be predicted from the pTR output SNR given in (31).

Equation (31) can be simplified since in (27) and (28) $C_{x2}(t_0,\tau) \ll \tau C_h$, $\sigma_w^2 = \sigma_u^2$, $\sigma_a^2/T_b \gg 1$, and $r_{p_4}(0) > r_{p_3}(0)$, such that $\sigma_{x2}^2(t_0,\tau) \ll \sigma_{x1}^2(t_0,\tau)$. Then (31) reduces to

$$SNR_{out}(t_0,\tau) \approx \frac{\sigma_y^2(t_0,\tau)}{\sigma_{x3}^2(\tau) + \sigma_{x1}^2(\tau)}, \tag{33}$$

and the approximation improves as τ increases, and more channel IR paths are included in the time window.

For values of $\tau > 0$ one can define

$$\Phi(t_0,\tau) = \frac{C_y(t_0,\tau)}{\tau^{\frac{1}{2}}}, \tag{34}$$

where $C_y(t_0,\tau)$ can be computed from (30) as

$$C_y(t_0,\tau) = \sum_{k=1}^{K} \int_{t_0}^{t_0+\tau} |h_k(t)|^2 dt, \tag{35}$$

that is the summation of the energy cumulative functions of the channels IRs at all hydrophones.

By using (34) in (33) it results that

$$\frac{SNR_{out}(t_0,\tau)}{\Phi^2(t_0,\tau)} = \frac{(\sigma_a^2/T_b) r_{p4}(0)}{\sigma_w^2 \sigma_u^2 K r_{p4}(0) + (\sigma_a^2/T_b)\sigma_u^2 C_h r_{p4}(0)}. \tag{36}$$

Since the right term of the equation is a constant in τ $SNR_{out}(t_0,\tau)$ and $|\Phi(t_0,\tau)|^2$ have the same shape and the optimum τ that guaranties the global maximum for $SNR_{out}(t_0,\tau)$ is given by

$$\tau_{opt} = \arg\max(\Phi(t_0,\tau)). \tag{37}$$

where, with no loss of generality, the time window starting point t_0 was considered to be chose arbitrarily before the main path arrivals of the $h_k(t)$ IRs. Equations (34) and (37) state the remarkable result that the time window that guarantees the pTR maximum output SNR does not depend on the noise power, and moreover that it only depends on the channel IRs (see (35)).

In a real situation $C_y(t_0,\tau)$ is not available since only a noisy version of $h_k(t)$ can be estimated in the pTR processor. An estimate of $\hat{C}_y(t_0,\tau)$ can be computed as

$$\begin{aligned}\hat{C}_y(t_0,\tau) &= \sum_{k=1}^{K}\int_{t_0}^{t_0+\tau} E\{|h_k(t)+u_k(t)|^2\}dt \\ &= C_y(t_0,\tau)+\sigma_u^2 K\tau, \end{aligned} \tag{38}$$

it results that

$$C_y(t_0,\tau) = \hat{C}_y(t_0,\tau) - \sigma_u^2 K\tau \tag{39}$$

where here $h_k(t)+u_k(t)$ is consider to be a narrowband estimate of the channel IRs. Replacing (39) in (34) yields an estimate of the optimal τ for real data

$$\begin{aligned}\hat{\Phi}(t_0,\tau) &= \frac{\hat{C}_y(t_0,\tau)-\sigma_u^2 K\tau}{\tau^{\frac{1}{2}}} \\ \hat{\tau}_{opt} &= \arg\max \hat{\Phi}(t_0,\tau) \end{aligned} \tag{40}$$

A sensitive estimate of $\hat{C}_y(t_0,\tau)$ should be used in (39) if good results using real data are expected. It will be seen in section IV. that when estimating $\hat{C}_y(t_0,\tau)$ with a single realization the estimate $\hat{\Phi}(t_0,\tau)$ becomes too sensitive to noise, but using mean values improves the quality of results.

III. Performance simulations in realistic channels

The simulation scenario comprises a range independent acoustic channel with 118 m depth, over a 1.5 m thick silt sub-bottom and a gravel like bottom. The sound speed profile is downward reflecting with a thermocline down to 30 meters and a sound speed ranging from 1500

m/s to 1510 m/s. The sound transmitter and the 16-hydrophone-4-meter-spaced receiving array were placed 1.3 km apart at respective depths of 74 and 30 m (first hydrophone). The transmitted data signal is a 2-PSK PAM signal with a 50% rolloff fourth-root raised-cosine pulse shape, the carrier frequency is 1600Hz, and the data rate is 300 bits/s.

The arrival pattern computed with the C-Snap normal mode model can be seen in figure 2, where the multipath spans over 100 ms, however with a higher concentration of energy in the first arrival paths. The main arrival path can be predicted by considering the maximum of the sum of all IR magnitudes. The beginning of the time window is set to two symbols before that maximum and the initial time window length is considered to be two symbols. The simulation results were computed by considering increments of half a symbol period in window duration τ.

Two cases will be under study: in the first case pTR will be applied to the arrival pattern of figure 2, such that the pTR output SNR is a convex function with a single maximum; in the second case the IRs of the 5 last hydrophones were intentionally delayed to generate a output SNR curve with two local maxima to test the time window length optimization with a non convex function.

Figure 4 shows the pTR output SNR (in dB) as a function of window length parameterized by the input SNR ($\mathrm{SNR_{in}}$), for the single maximum case (a) and the double maximum case (b). In each case, results are shown via Monte-Carlo simulation ('o'), using the closed form expression (31) ('∇') and the MSE-based form (32) ('$\Box$'). Figure 4(a) shows that for a low SNR_{in} good agreement is obtained between the three curves. For high SNR_{in} the residual ISI of the TR operator becomes dominant and leads to saturation of SNR_{mse}. Despite these differences it should be noted that the maxima are always obtained for the same time window length, which means that the optimum time window length predicted by the theoretical expression (37) fully coincides with the simulations. Similar observations can be made for figure 4(b) where the output SNR curve exhibit tow local maxima.

Figure 5 shows the behavior of $\Phi(t_0, \tau)$ given by (37) versus time window length: single maximum case (a) and two maxima case (b). It can be seen that, as predicted by the theoretical derivation, the maxima clearly coincide with those of SNR_{out} in figure 4 both for the single maximum (a) and double maxima (b) cases.

IV. Experimental results

The experimental data were acquired during the INTIFANTE'00 sea trial that took place off the town of Setúbal, approximately 50km south of Lisbon (Portugal) in October 2000 [17]. This paper concentrates on the Binary Phase Shift Keying data collection. The scenario was similar to that used in section III. with the main differences being that with real data there will be noise corruption and geometric/environment mismatch between the probe-signal and the data transmissions. The acoustic source was suspended from a free drifting oceanographic vessel - NRP D. Carlos I - at a nominal depth of 60 m. The receiver was a surface suspended 16-equispaced-hydrophone vertical line array spanning nominal depths between 31 an 91 m. The source range distance was approximately 1420 m $\pm$ 100 m. Nine sequential transmissions (in the following referred to as shot 1 to 9) will be considered, each one composed of a probe-signal transmitted 0.5 seconds before a 5 second PSK data stream, with a repetition rate of 7 seconds.

During the INTIFANTE'00 sea trial the pTR based data communications system was similar to that of figure 1, with the $p_2(t)$ narrowband filter of the IR estimation operation (path above in figure 1) distributed between the transmitter and the receiver, i.e., the transmitted probe-signal was a fourth-root raised-cosine pulse and IR estimates were obtained by correlating the received probe-signal with the transmitted one (see [8] for details).

The estimated arrival pattern for shot 9 can be seen in figure 3. This figure shows a number of arrival paths that are not as well defined as in the simulations due to noise corruption. Such noise corruption will, obviously, affect the proposed time window optimization method

given by equation (40) since $\hat{C}_y(t_0, \tau)$ in (38) has to be computed from a single realization of $|h_k(t) + u_k(t)|^2$. In (40) the noise variance σ_u^2 was calculated considering the mean of the noise variances for all hydrophones.

Figure 6(a) shows the pTR output SNR computed via the MSE at the detector input with (32), for the first 3 seconds of data during shot 9. One can see a progressive degradation in performance due to geometric/environmental mismatch in IRs between the probe-signal and data-signal transmissions. Such loss of performance affects primarily larger time windows since those include the later arrivals that are usually considered more prone to fading. Despite this channel variability, figure 6(b) shows that the predicted pTR output SNR maxima, given by the local maxima of $\hat{\Phi}(t_0, \tau)$, are in a good agrement with the true local maxima in the first-second curve of figure 6(a). Although the maxima location are well predicted the first and the second maxima are interchanged.

Figure 7 shows analogous results for shot 7. Figure 7(a) shows that, although this case presents a pTR output SNR maxima location almost constant during the three seconds of data only the first maximum is predicted by the $\hat{\Phi}(t_0, \tau)$ curve in figure 7(b).

Figure 6 and 7 present tow extreme cases in the pTR output SNR maxima detection: in the former the global maximum is predicted to be the second true maximum but a reasonable shape agreement is observed between $\hat{\Phi}(t_0, \tau)$ and the first-second SNR_{out} curves; while in the later the global maxima is well predicted but a different shape is observed for the two curves. Typically the other shots present an intermediate behavior between shot 7 and 9.

To verify the robustness of the proposed optimization technique a mean analysis over the first second of data using all nine shots is presented in figure 8. The continuous line shows that the mean pTR SNR_{out} will partially eliminate the fake (noise-induced) paths and the later path arrivals that are more sensitive to fading. The dashed line shows the mean of $\hat{\Phi}(t_0, \tau)$ over all shots. One can see that these two curves are in excellent agreement and display an almost constant ratio, such that the same maxima locations are predicted. That

suggests that pTR performance is strongly affected by channel noise that will introduce a fake path structure. The problem can be overcome by enhanced IR estimation using large time-bandwidth product probe-signal or by averaging a number of closely time spaced probe-signals sent before the data stream.

V. Conclusion and future work

The problem of time window optimization when operating a pTR with a vertical line array for underwater communications was considered. It was found that the optimum time window simultaneously guarantees higher pTR output SNR and lower MSE at the slicer/detector input. Time window optimization was made possible by the derivation of a closed-form expression for the pTR output SNR (31). Such expression allow the derivation of (37) that clearly states that the optimum time window depends only on the channel IRs and it is not dependent on the data signal or noise level. Simulation results confirm and gauge for the theoretic foresight.

When applied to real data the channel IRs are not available and noisy estimates must be used. Even with heavily noise corrupted IRs the developed technique presents a good fit with the pTR output SNR and its global maximum being closely predicted in most of the shots. Noise-related problems in IRs estimation are mainly due (in real data) to the use of low power probe-signals (fourth-root raised cosine pulse). The usage of high power probe-signals such as chirp signals or M-sequences should be addressed in future experiments. Despite its quality, it was found that the optimum time window loses validity after only a few seconds due to geometric/environment variability. Future developments should address the problem of a real time estimation of the optimum time window.

Although it was developed for pTR, the time window optimization method can also be applied to aTR by considering that in the later case the noise term $x3$ does not exist and $x2$ and $x1$ (10) are slightly different (see [5]).

Acknowledgments

The authors would like to thank the NATO Undersea Research Centre (NURC) for the loan of the acoustic sound source, the support of Enrico Muzzi and the NRP D. Carlos I crew during the INTIFANTE'00 sea trial. This work was financed by FCT, Portugal, under NUACE project, contract POSI/CPS/47824/2002, ATOMS project, contract POCTI/P/MAR/15296/1999, and the Portuguese Ministery of Defense under the LOCA-PASS project.

A Deterministic and stochastic filters autocorrelation

This appendix recalls the autocorrelation of the response Y, of a finite impulse response filter H, to an input signal X when input and filter autocorrelations are known and when: case 1 - H is stochastic and X is stochastic ; case 2 - H is deterministic and X is stochastic; case 3 - H is stochastic and X is deterministic. The filter output is given by the convolution

$$Y(t) = \int_{-\infty}^{+\infty} H(t-u)X(u)du, \tag{A2}$$

and the filter output autocorrelation

$$\begin{aligned} R_Y(t+t',t) &= E\{Y(t+t')Y(t)\} \\ &= \int\int E\{H(t+t'-u)H(t-v)\}E\{X(u)X(v)\}dudv \\ &= \int\int E\{X(t+t'-u)X(t-v)\}E\{H(u)H(v)\}dudv, \end{aligned} \tag{A3}$$

since X and H are independent, (A3) is valid for H and X deterministic or stochastic. In the following it will be use the index t_0, τ to represent a signal time limited by the unit-gate function

$$\Pi_\tau(t-t_0) = \Pi_{t_0,\tau}(t) = \begin{cases} 1, & t_0 \le t < t_0+\tau \\ 0, & \text{other } t \end{cases} . \tag{A4}$$

Capital letters designate stochastic quantities and lower case designate deterministic quantities, thus R will represent the stochastic autocorrelation and r the deterministic autocorrelation.

In case 1 H_τ is a stochastic time limited signal (where t_0 has been dropped since in a stochastic signal the instant when the unit-gate function is applied is irrelevant), and X an unlimited WSS stochastic signal, the output filter autocorrelation as given in [18], is equal to

$$R_Y(t') = E\{r_{H,\tau}(t')\} * R_X(t'), \tag{A5}$$

where

$$E\{r_{H,\tau}(t')\} = E\left\{\int H_\tau(t+t')H_\tau(t)dt\right\}. \tag{A6}$$

Considering that the time limited stochastic process H_τ is the result of the product of a WSS process H, with a rectangular window (A4)

$$E\{r_{H,\tau}(t')\} = R_H(t')\tau\Delta_\tau(t'), \tag{A7}$$

where $\tau\Delta_\tau(t')$ is the triangular function that results from the deterministic autocorrelation of the rectangular function (A4). When X and H are both white gaussian processes with autocorrelations $\sigma_X^2\delta(t')$ and $\sigma_H^2\delta(t')$ respectively the output autocorrelation will be given by

$$R_Y(t') = \sigma_X^2\sigma_H^2\tau r_\delta(t'), \tag{A8}$$

and Y is a white stochastic signal, since $r_\delta(t') = \delta(t') * \delta(t')$ is the autocorrelation of the dirac impulse.

Case 2 is a standard case where $h_{t_0,\tau}$ is a deterministic signal that results from the product of an infinite signal with time window (A4) applied in the arbitrary instant t_0, and X is an infinite stochastic signal. The output filter autocorrelation is given by

$$R_Y(t') = r_{h,t_0,\tau}(t') * R_X(t'), \tag{A9}$$

where

$$r_{h,t_0,\tau}(t') = \int h_{t_0,\tau}(t+t')h_{t_0,\tau(t)}dt \tag{A10}$$

$$= \begin{cases} \int_{t_0}^{t_0+\tau-t'} h(w+t')h(w)dw, & \tau \geq t' > 0 \\ \int_{t_0}^{t_0+\tau} h(w+t')h(w)dw, & t' = 0 \\ \int_{t_0-t'}^{t_0+\tau} h(w+t')h(w)dw, & 0 > t' \geq -\tau \\ 0, & \text{other } t' \end{cases} \tag{A11}$$

When $h_{t_0,\tau}$ is a deterministic signal and X is an infinite white gaussian process

$$R_Y(t') = \sigma_X^2 r_{h,t_0,\tau}(t'). \tag{A12}$$

and the filter output Y is a WSS stochastic signal.

In case 3 x is deterministic, and H_τ a time limited stochastic signal that, as in case 1, results from the product of a WSS signal with the rectangular window (A4), since the signal is WSS the moment when the window is applied is not important and t_0 can be dropped. In that condition, since

$$E\{H_\tau(u)H_\tau(v)\} = R_H(u-v)[\Pi_\tau(u)\Pi_\tau(v)], \tag{A13}$$

equation (A3) becomes

$$R_Y(t+t',t) = \int\int [x(t+t'-u)x(t-v)][\Pi_\tau(u)\Pi_\tau(v)]R_H(u-v)dudv, \tag{A14}$$

if we change the independent variables

$$\begin{cases} w = t - v \\ t - u = w - z \end{cases}, \tag{A15}$$

the output autocorrelation becomes

$$R_Y(t+t',t) = \int R_H(z)A_\tau(t',t,z)dz, \tag{A16}$$

with

$$A_\tau(t',t,z) = \int [x(w-z+t')\Pi_\tau(t-w+z)][x(w)\Pi_\tau(t-w)]dw. \tag{A17}$$

Equation (A17) can be rewriten in four intervals defined by variable z

$$A_\tau(t',t,z) = \begin{cases} \int_{t-\tau}^{t+z} x(w-z+t')x(w)dw, & -\tau \le z < 0 \\ \int_{t-\tau}^{t} x(w-z+t')x(w)dw, & z = 0 \\ \int_{t-\tau+z}^{t} x(w-z+t')x(w)dw, & 0 < z \le \tau \\ 0, & \text{others} \end{cases} . \tag{A18}$$

When x is deterministic and H is a time limited white gaussian process with auto-correlation given by $\sigma_H^2\delta(t')$ the auto-correlation of Y becomes

$$R_Y(t+t',t) = \sigma_H^2 A_\tau(t',t,z=0). \tag{A19}$$

that is a non stationary stochastic signal.

B Time windowed passive Time Reversal

Without mismatch pTR operation consists (up to a constant time delay) on the sum over all hydrophones of the deterministic correlation between the two subsequent IRs, that is

$$P_{TR}(t) = \sum_{k=1}^{K} h_k(t) * h_k(-t). \tag{A20}$$

In the frequency domain (where pTR is usually termed passive phase conjugation) the same result is attained by

$$\begin{aligned} P_{PC}(\omega) &= \sum_{k=1}^{K} H_k(\omega)H_k^*(\omega) \\ &= a_k^2 \sum_{n=1}^{M}\sum_{m=1}^{M} \Psi_n(\zeta_0)\Psi_m(\zeta_0)\frac{e^{j(\xi_n-\xi_m^*)R}}{\sqrt{\xi_n\xi_m^*}} \sum_k \Psi_n(\zeta_k)\Psi_m(\zeta_k) \\ &= a_k^2 \sum_{m=1}^{M} |\Psi_m(\zeta_0)|^2 \frac{e^{j(\xi_m-\xi_m^*)R}}{\sqrt{\xi_m\xi_m^*}} \\ &= a_k^2 \sum_{m=1}^{M} |\Psi_m(\zeta_0)|^2 \frac{e^{-2Im(\xi_m)R}}{|\xi_m|} \\ &\approx C \end{aligned} \tag{A21}$$

where all terms have obvious notations in the normal mode formulation of the acoustic field. The modes orthogonality property was used, in a similar manner to [19] for pTR and to [11]

for aTR. In (A21) the $Im(\xi_m)$ exponential, according to [19], acts to attenuate higher order modes and higher frequencies. It results that $P_{PC}(\omega) \approx C$ is approximately constant over the narrowband frequencies of interest and in the time domain $P_{TR}(t)$ will be a *sinc* function convolved with a weighted dirac proportional to C.

The time windowing operation consists in multiplying the IRs $h_i(t)$ by a unit-gate function $\Pi_{t0,\tau}(t)$, given in (A4), with starting time t_0 and length τ. By considering the ray mode approximation [20, 21] where at a given frequency, higher order modes are associated with later rays, the effect of a time window that eliminates later rays can be reversed to mode analysis where it will filter out higher order modes. In the following it will be considered that $Me(t_0, \tau)$ is the set of modes that have not been filtered by the time window

The influence of the time windowing operation over the pTR processor can now be considered under two aspects: when both subsequent probe-signals are time limited or when only one of them is time limited. In the first case the resulting P_{PC} will be given by

$$\begin{aligned} P_{PC,2tw}(\omega) &= \sum_{k=1}^{K} H_{k,t_0,\tau}(\omega) H^*_{k,t_0,\tau}(\omega) \\ &= a_k^2 \sum_{n=1}^{Me(t_0,\tau)} \sum_{m=1}^{Me(t_0,\tau)} \Psi_n(\zeta_0)\Psi_m(\zeta_0) \frac{e^{j(\xi_n - \xi_m^*)R}}{\sqrt{\xi_n \xi_m^*}} \sum_k \Psi_n(\zeta_k)\Psi_m(\zeta_k) \\ &= a_k^2 \sum_{m=1}^{Me(t_0,\tau)} |\Psi_m(\zeta_0)|^2 \frac{e^{-2Im(\xi_m)R}}{|\xi_m|} \\ &\approx C' \end{aligned} \tag{A22}$$

In the second case the resulting P_{PC} will be given by

$$\begin{aligned} P_{PC,1tw}(\omega) &= \sum_{k=1}^{K} H_k(\omega) H^*_{k,t_0,\tau}(\omega) \\ &= a_k^2 \sum_{n=1}^{M} \sum_{m=1}^{Me(t_0,\tau)} \Psi_n(\zeta_0)\Psi_m(\zeta_0) \frac{e^{j(\xi_n - \xi_m^*)R}}{\sqrt{\xi_n \xi_m^*}} \sum_k \Psi_n(\zeta_k)\Psi_m(\zeta_k) \\ &= C' + a_k^2 \sum_{n=Me(t_0,\tau)}^{M} \sum_{m=1}^{Me(t_0,\tau)} (\cdot) \\ &\approx C'' \end{aligned} \tag{A23}$$

With $C' \equiv C''$ only if the TR associated assumption is accomplished. As the time window increases $Me(t_0, \tau)$ converges to $M(\omega)$ and, C' and C'' converge to C.

References

[1] M. Stojanovic, J. Catipovic, and J. Proakis. Adaptive multichannel combining and equalization for underwater acoustic communications. *J. Acoust. Soc. America*, 94(3):1621–1631, 1993.

[2] R.D. Jackson and R.D. Dowling. Phase conjugation in underwater acoustics. *J. Acoust. Soc. Am.*, 89(1):171–181, January 1991.

[3] R.D. Dowling. Acoustic pulse compression using passive phase-conjugate processing. *J. Acoust. Soc. America*, 95(3):1450–1458, 1994.

[4] A. Silva, S. Jesus, J. Gomes, and V. Barroso. Underwater acoustic communications using a 'virtual' electronic time-reversal mirror approach. In P. Chevret and M.Zakharia, editors, *5th European Conference on Underwater Acoustics*, pages 531–536, Lyon, France, June 2000.

[5] J. Gomes and V. Barroso. Asymmetric underwater acoustic communication using a time-reversal mirror. In *Proc. of the MTS/IEEE Oceans 2000*, Providance, USA, 2000.

[6] D. Rouseff, L.J.W. Fox, D. Jackson, and D.C. Jones. Underwater acoustic communications using passive phase conjugation. In *Proc. of the MTS/IEEE Oceans 2001*, pages 2227–2230, Honolulu, Hawai, USA, November 2001.

[7] S.M. Jesus and A.J. Silva. Time reversal and spatial diversity: issues in a time varying geometry test. In Siderius Porter and Kuperman, editors, *Proc. Conf. on High Frequency Ocean Acoustics*, pages 530–538, La Jolla, USA, March 2004.

[8] A. Silva and S. Jesus. Underwater communications using virtual time-reversal in a variable geometry channel. In *Proc. MTS/IEEE Oceans'2002*, pages 2416–2421, Biloxi, USA, November, 2002.

[9] T. C. Yang. Differences between passive-phase conjugation and decision-feedback equalizer for underwater acoustic communications. *IEEE Journal of Oceanic Engineering*, 29(2):472–487, April 2004.

[10] M. Stojanovic. Retrofocusing techniques for high rate acoustic communications. *J. Acoust. Soc. America*, 117(3):1173–1185, 2005.

[11] W.A. Kuperman, W. Hodgkiss, H. Chung Song, T. Akal, C. Ferla, and D. Jackson. Phase conjugation in the ocean: Experimental demonstration of an acoustic time-reversal mirror. *J. Acoust. Soc. Am.*, 103(1):25–40, January 1998.

[12] J. Gomes, A. Silva, and S. Jesus. Joint passive time reversal and multichannel equalization for ubderwater communications. In *Proc. of the MTS/IEEE Oceans'06*, Boston, MA, USA, September 2006.

[13] G.F. Edelmann, W.S. Hodgkiss, S. Kim, W.A. Kuperman, H.C. Song., and T. Akal. Underwater acoustic communications using time-reversal. In *Proc. of the MTS/IEEE Oceans 2001*, pages 2231–2235, Honolulu, Hawai, USA, 5-8 November 2001.

[14] J.V. Candy, A.M. Meyer, A.J. Poggio, and B.L. Guidry. Time-reversal processing for an acoustic communications experiment in a highly reverberant environment. *J. Acoust. Soc. America*, 115(4):1621–1631, 2004.

[15] E.A. Lee and D.G. Messerschmitt. *Digital Communication*. Kluwer Academic Publishers, Massachusetts, 1994.

[16] J.G. Proakis. *Digital Communications*. McGraw-Hill, Massachusetts, 1995.

[17] S.M. Jesus and A. Silva. Virtual time reversal in underwater acoustic communications: Results on the intifante'00 sea trial. In *Proc. of Forum Acusticum*, Sevilla, Spain, September 2002.

[18] W.A. Gardner. A new method of channel identification. *IEEE Trans. Communications*, 39:813–817, 1991.

[19] D. Rouseff, D.R. Jackson, W.L.J. Fox, D.C. Jones, J.A. Ritcey, and D.R. Dowling. Underwater acoustic communications by passive-phase conjugation: Theory and experimental results. *J. Oceanic Engineering*, 26(4):821–831, 2001.

[20] I. Tolstoy and C.S. Clay. *Ocean Acoustics: Theory and experiments in underwater sound*. AIP, New York, 1966.

[21] D.M.F. Chapman and Dale D. Ellis. The group velocity of normal modes. *J. Acoust. Soc. America*, 3(74):973–979, September 1983.

Figure captions

Figure 1: Block-diagram for the application of passive time reversal to digital communications.

Figure 2: Simulated depth dependent impulse responses over a realistic scenario: start time '0', optimum window duration '*' and maximum window duration '+'.

Figure 3: Real data estimated vertical array estimated impulse responses: start time '0', optimum window duration '*' and maximum window duration '+'.

Figure 4: Simulated pTR output SNR for the single maximum case (a), and for the two local maxima case (b).

Figure 5: Simulated performance of the proposed optimal time window prediction method by using (34) and (37): maximum prediction for the single maximum case (a) and maxima prediction for the two local maxima case (b).

Figure 6: Real data performance of the proposed optimal time window prediction method obtained in shot 9: pTR output SNR computed by using the MSE at the slicer/detector input (a) and maxima prediction by using (40) (b).

Figure 7: Real data performance of the proposed optimal time window prediction method obtained in shot 7: pTR output SNR computed by using the MSE at the slicer/detector input (a) and maxima prediction by using (40) (b).

Figure 8: Mean analysis over all shots for the real data performance of the proposed optimal time window prediction method: pTR output SNR output computed by using the shot-mean MSE at the slicer/detector input (a) and shot-mean of the maxima prediction by using (40) (b).

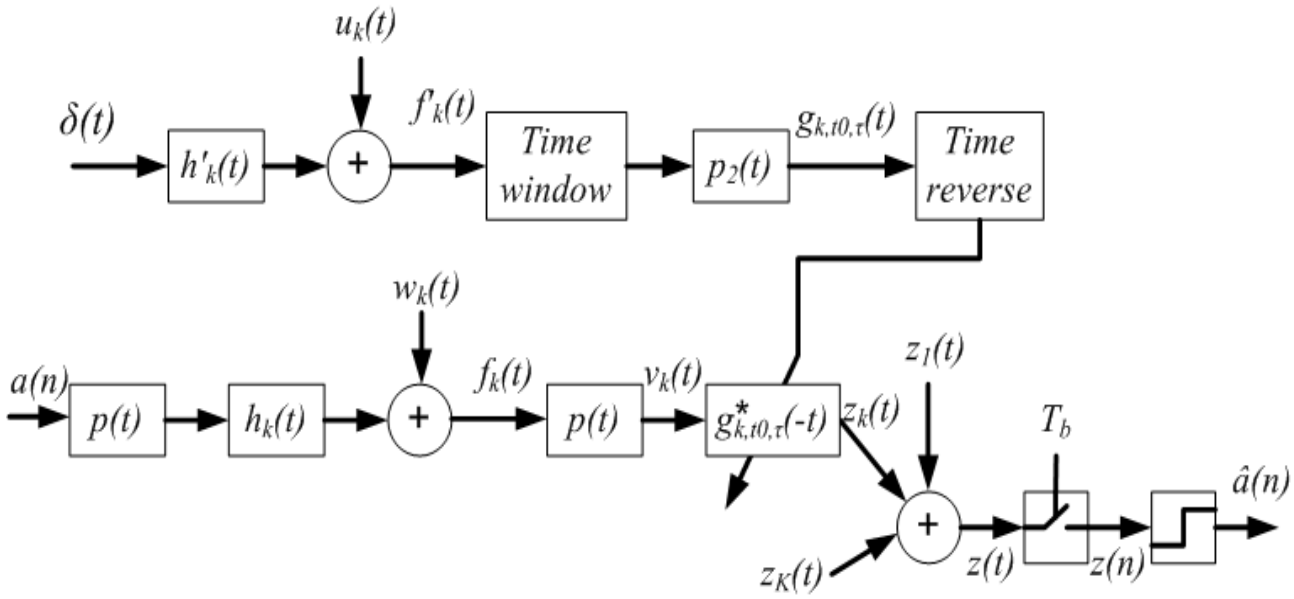
$u_k(t)$
$\delta(t)$
$h'_k(t)$
$f'_k(t)$
Time window
$p_2(t)$
$g_{k,t0,\tau}(t)$
Time reverse
$w_k(t)$
$a(n)$
$p(t)$
$h_k(t)$
$f_k(t)$
$p(t)$
$v_k(t)$
$g^*_{k,t0,\tau}(-t)$
$z_k(t)$
$z_1(t)$
T_b
$\hat{a}(n)$
$z_K(t)$
$z(t)$
$z(n)$

Figure 1:

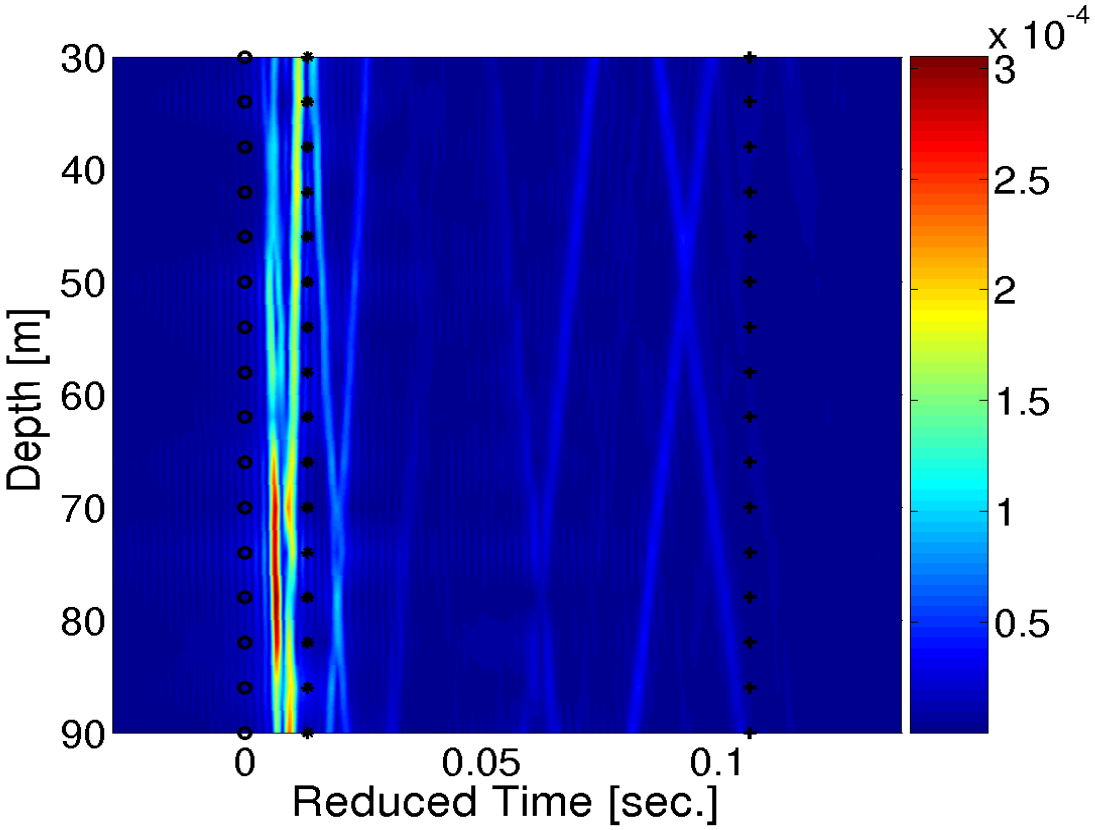
x 10^-4
3
2.5
2
1.5
1
0.5
30
40
50
60
70
80
90
Depth [m]
0
0.05
0.1
Reduced Time [sec.]

Figure 2:

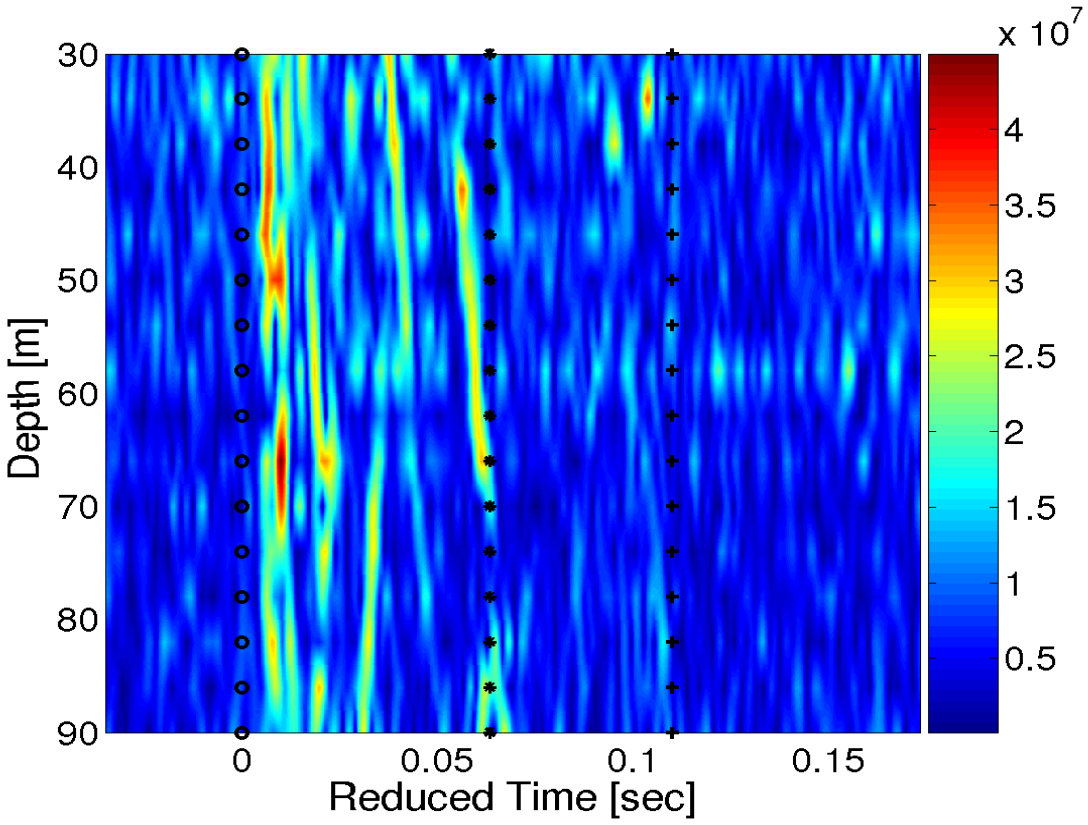
x 10^7
4
3.5
3
2.5
2
1.5
1
0.5
30
40
50
60
70
80
90
Depth [m]
0
0.05
0.1
0.15
Reduced Time [sec]

Figure 3:

(a)

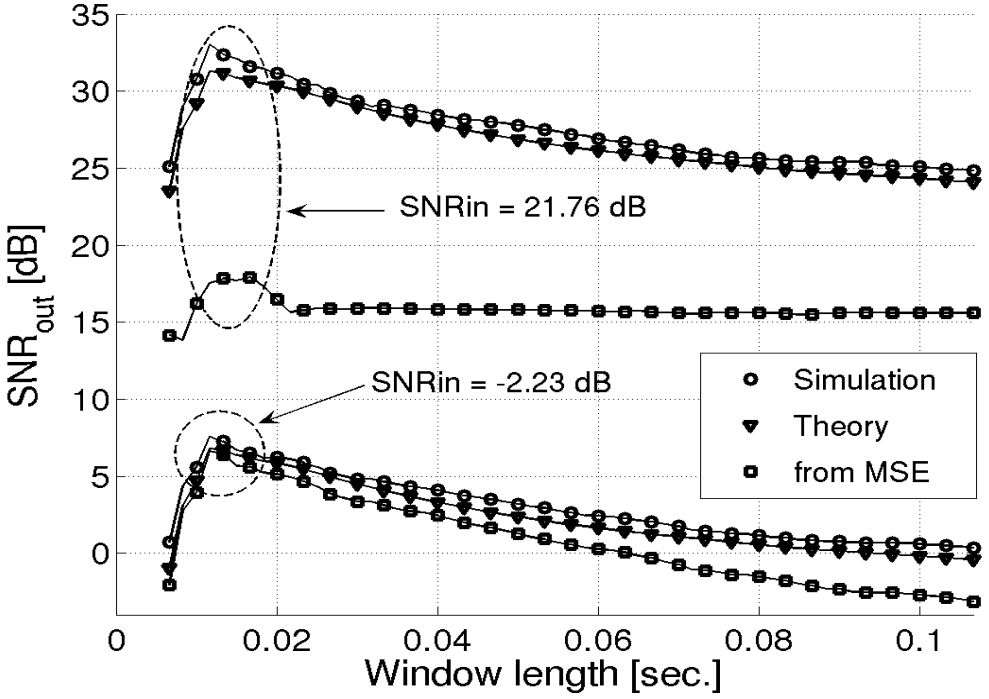
SNRout [dB]
Window length [sec.]
SNRin = 21.76 dB
SNRin = -2.23 dB
Simulation
Theory
from MSE

(b)

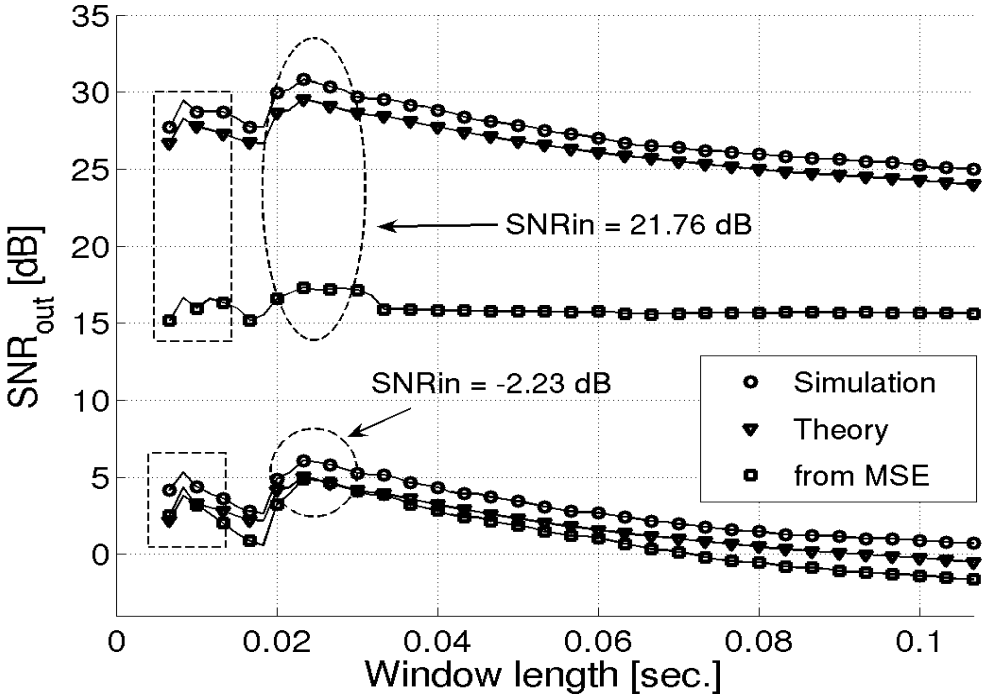
SNRout [dB]
Window length [sec.]
SNRin = 21.76 dB
SNRin = -2.23 dB
Simulation
Theory
from MSE

Figure 4:

(a)

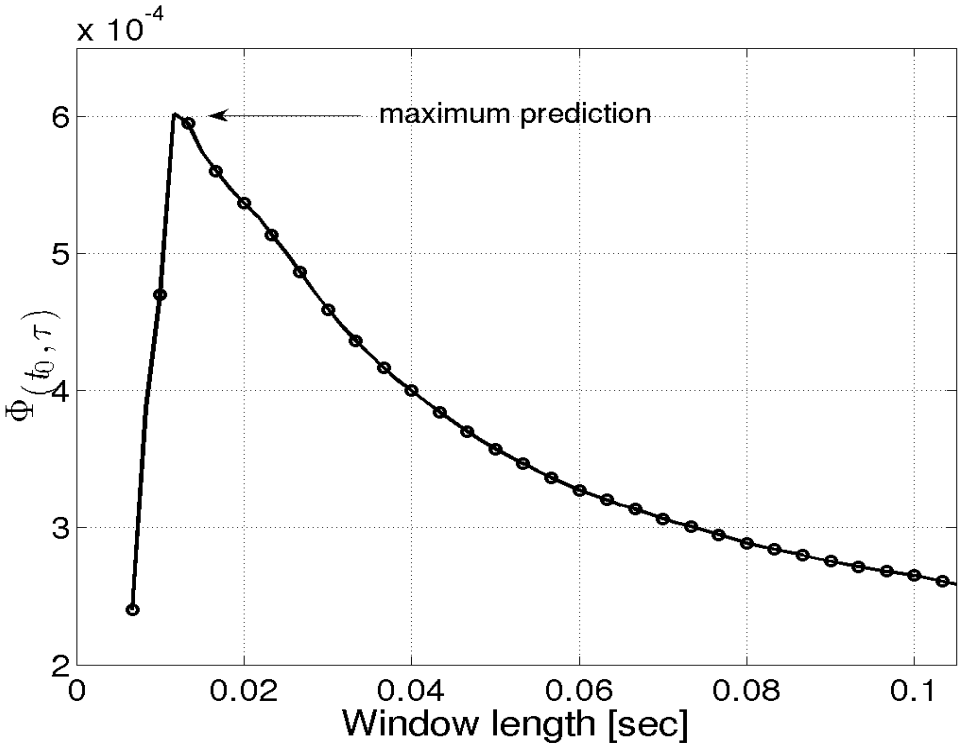
x 10^-4
maximum prediction
Φ(t0,τ)
Window length [sec]
0
0.02
0.04
0.06
0.08
0.1
2
3
4
5
6

(b)

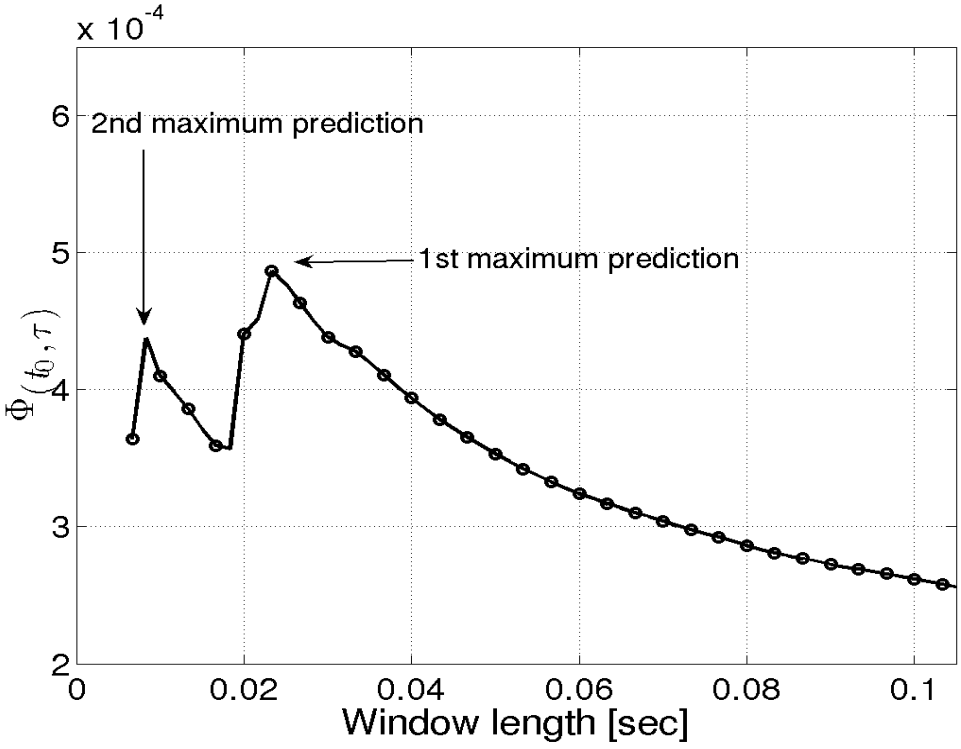
x 10^-4
2nd maximum prediction
1st maximum prediction
Φ(t0,τ)
Window length [sec]
0
0.02
0.04
0.06
0.08
0.1
2
3
4
5
6

Figure 5:

(a)

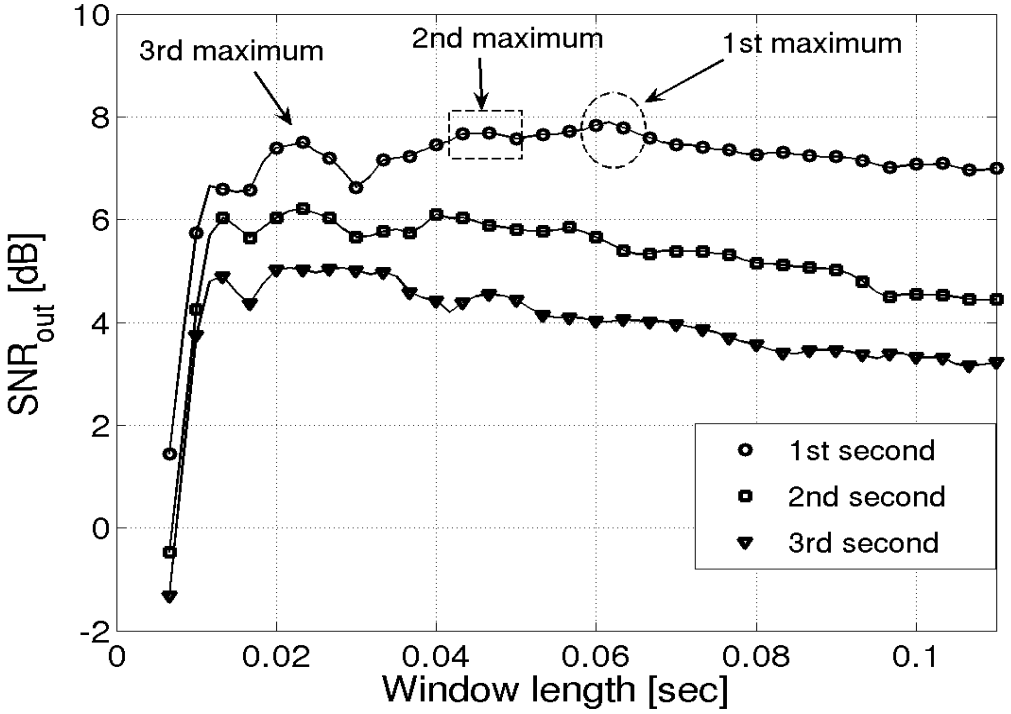
3rd maximum
2nd maximum
1st maximum
SNR_out [dB]
Window length [sec]
1st second
2nd second
3rd second

(b)

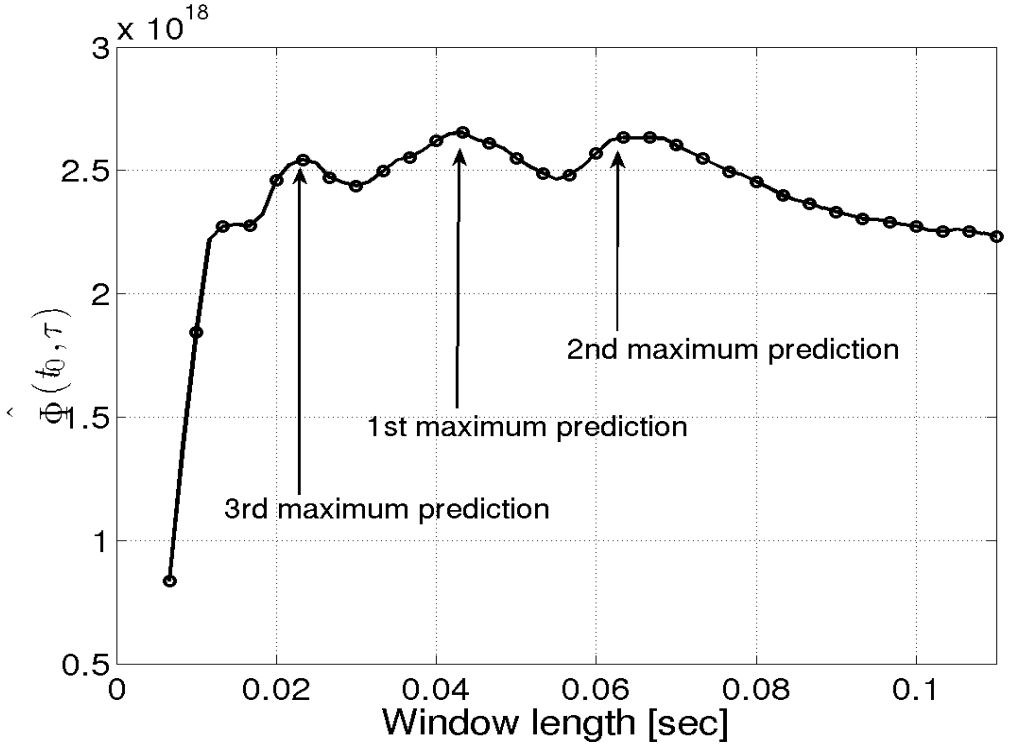
x 10^18
Φ̂(t0,τ)
Window length [sec]
2nd maximum prediction
1st maximum prediction
3rd maximum prediction

Figure 6:

(a)

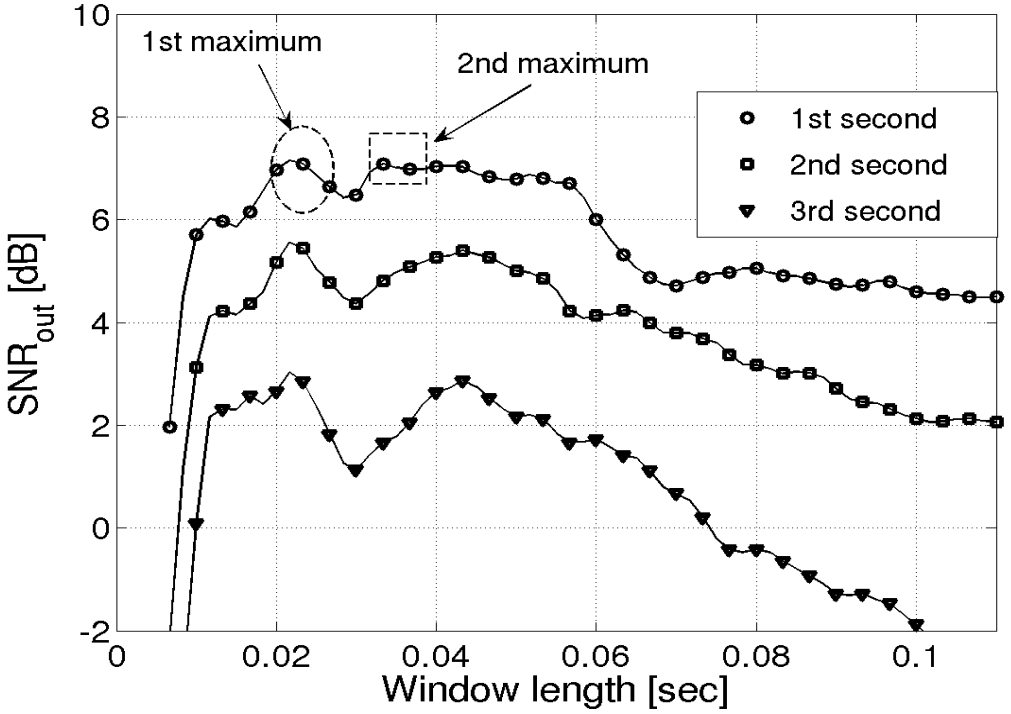
1st maximum
2nd maximum
1st second
2nd second
3rd second
SNR_out [dB]
Window length [sec]

(b)

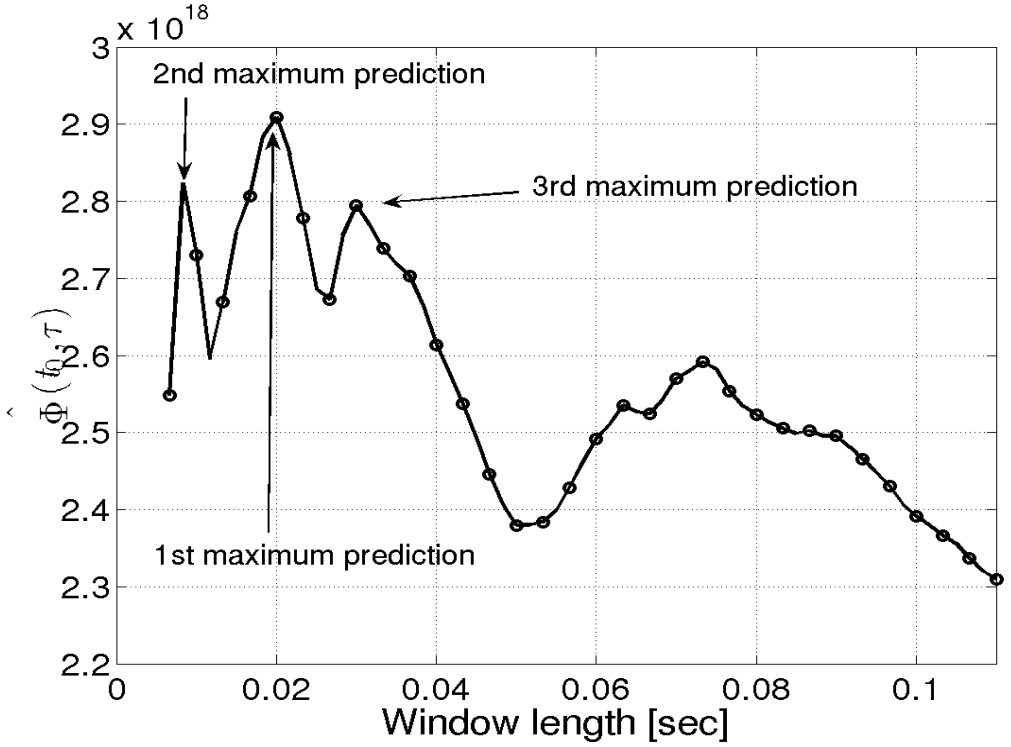
x 10^18
2nd maximum prediction
3rd maximum prediction
1st maximum prediction
Window length [sec]

Figure 7:

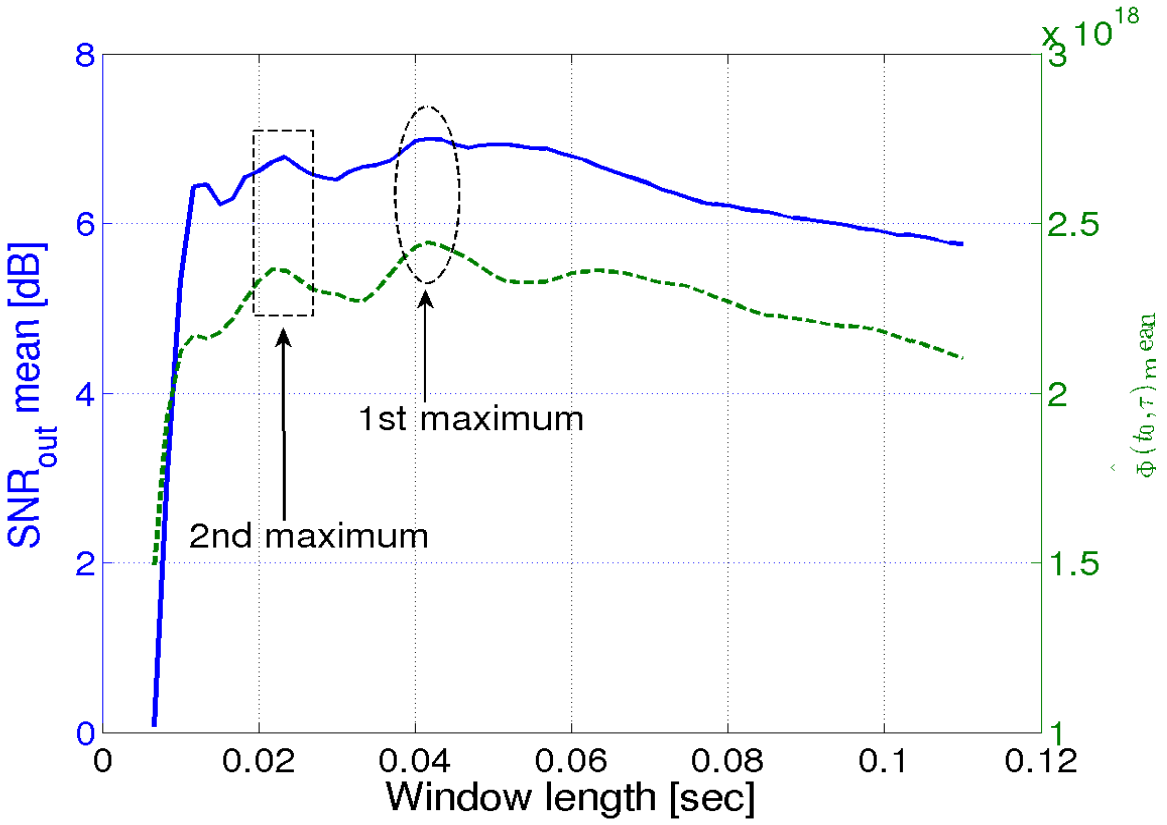
x 10^18
SNR_out mean [dB]
Φ̂(t0,τ) mean
1st maximum
2nd maximum
Window length [sec]
0
2
4
6
8
1
1.5
2
2.5
3
0.02
0.04
0.06
0.08
0.1
0.12

Figure 8: